JACS
JOURNAL OF THE AMERICAN CHEMICAL SOCIETY
Article
pubs.acs.org/JACS

Liposomal Texaphyrin Theranostics for Metastatic Liver Cancer

Min Hee Lee,[*,†] Eun-Joong Kim,[‡,§] Hyunseung Lee,[‡,∥] Hyun Min Kim,[‡,∥] Min Jung Chang,[†] Sun Young Park,[†] Kwan Soo Hong,[*,‡,∥] Jong Seung Kim,[*,⊥] and Jonathan L. Sessler[*,#]

[†]Department of Chemistry, Sookmyung Women's University, Seoul 04310, Korea
[‡]Bioimaging Research Team, Korea Basic Science Institute, Cheongju 28119, Korea
[§]Department of Biomedical Engineering, School of Medicine, Kyung Hee University, Seoul 02447, Korea
[∥]Immunotherapy Convergence Research Center, Korea Research Institute of Bioscience and Biotechnology, Daejeon 34141, Korea
[⊥]Department of Chemistry, Korea University, Seoul 02841, Korea
[#]Department of Chemistry, University of Texas at Austin, Austin, Texas 78712-1224, United States

Supporting Information

ABSTRACT: Reported here is a new theranostic agent, **1**, which consists of a Gd^{3+}-texaphyrin core conjugated to a doxorubicin prodrug via a disulfide bond. Conjugate **1** was designed to undergo cleavage in the presence of glutathione (GSH), a species typically upregulated in cancer cells. As prepared, conjugate **1** displays no appreciable fluorescence. However, when exposed to excess GSH an increase in the fluorescence intensity at 592 nm is observed that is ascribed to release of free doxorubicin. To improve the solubility and enhance the tumor targeting of **1**, it was loaded into folate-receptor-targeted liposomes to produce **FL-1** (for folate liposome loaded with **1**). As inferred from both fluorescence turn on studies and independent HPLC analyses, **FL-1** was found to undergo selective uptake and cleavage to release free Dox in the KB and CT26 cell lines, which express folate receptors on the cell surface, relative to the HepG2 and NIH3T3 cell lines, which show low expression of those receptors. **FL-1** was found to produce a greater antiproliferative effect in the case of the KB and CT26 cell lines as compared to that in the HepG2 and NIH3T3 cell lines. **FL-1** was also found to provide enhanced magnetic resonance imaging in vivo under conditions of T_1 contrast in the early stage of metastatic cancer progression. Finally, time-dependent tumor regrowth studies involving both subcutaneous and metastatic liver cancer mouse models revealed that **FL-1** is capable of reducing the tumor burden in vivo.

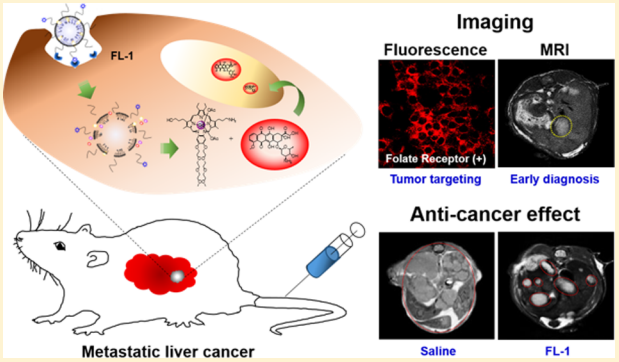

INTRODUCTION

Metastatic liver cancer is more prevalent than primary liver cancer but no less pernicious.[1,2] Liver metastases commonly arise from gastrointestinal cancers, including those of the esophagus, stomach, pancreas, and colon, as well as from other solid cancers.[3] The early diagnosis and accurate characterization of metastatic lesions is crucial to determining the prognosis of the patient and making proper therapeutic decisions. Magnetic resonance imaging (MRI) is a particularly useful noninvasive technique that is widely used to visualize and evaluate hepatic metastases.[3,4] Liver-specific magnetic resonance (MR) contrast agents based on gadolinium chelates have been developed that are capable of providing the enhanced lesion-to-liver images.[5] Recently, fluorescence imaging using small molecules, e.g., indocyanine green (ICG), has been applied to liver cancer visualization and fluorescence-guided surgery.[6,7] MR imaging provides good spatial resolution and soft tissue contrast, while fluorescence imaging is characterized by high sensitivity and provides valuable information on the local cellular level.[8,9] We believe that the combination of MR and fluorescence imaging could provide synergistic advantages over either modality alone. Particularly attractive would be agents that permit diagnosis via both these complementary techniques while providing a therapeutic benefit. Here, we report an example of such a dual detection theranostic agent. It is based on a combination of a gadolinium (Gd^{3+}) texaphyrin and a doxorubicin cytotoxin. As detailed below, this agent allows liver cancer imaging in both subcutaneous and metastatic liver cancer murine models while reducing the cancer burden as inferred from tumor regrowth studies.

Theranostics are systems that permit diagnostic imaging while providing a potential therapeutic benefit. This is a very active area of research, and currently, theranostics are being developed for use in a number of disease targets.[10−12] Many of own efforts have entered on the development of cleavable linker-based multifunctional conjugates for targeted cancer drug delivery and fluorescence-based imaging.[13−15] A number of the

Received: September 16, 2016
Published: November 22, 2016

DOI: 10.1021/jacs.6b09713
J. Am. Chem. Soc. 2016, 138, 16380−16387

Scheme 1. Structures of Conjugates and Liposomes and Schematics of Mechanism and Liver Cancer Models Used[a]

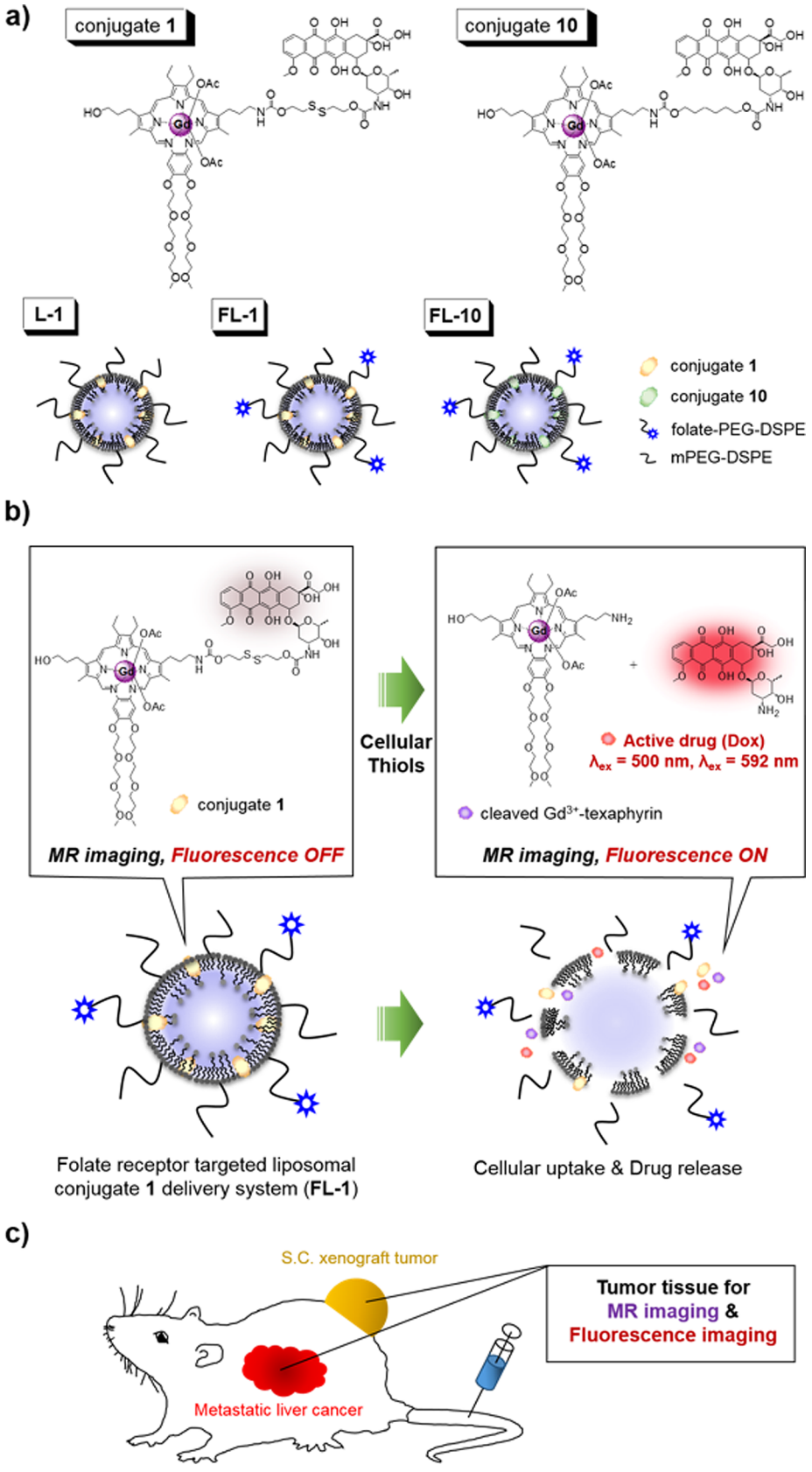

[a](a) Structures of conjugates **1** and **10** and liposomes **L-1**, **FL-1**, and **FL-10** used in this study. (b) Schematic illustration of the proposed Dox release and fluorescence enhancement produced by **FL-1** upon exposure to cellular thiols. (c) Subcutaneous (s.c.) xenograft tumor and metastatic liver cancer models prepared using the KB and CT26 cell lines, respectively. Proposed accumulation of free Dox in the resulting cancerous lesions after administration of **FL-1** via tail-vein injection and conjugate cleavage is also shown, as are the two potential modes of tumor imaging.

DOI: 10.1021/jacs.6b09713
J. Am. Chem. Soc. 2016, 138, 16380−16387

Scheme 2. Synthesis of Conjugate 1[a]

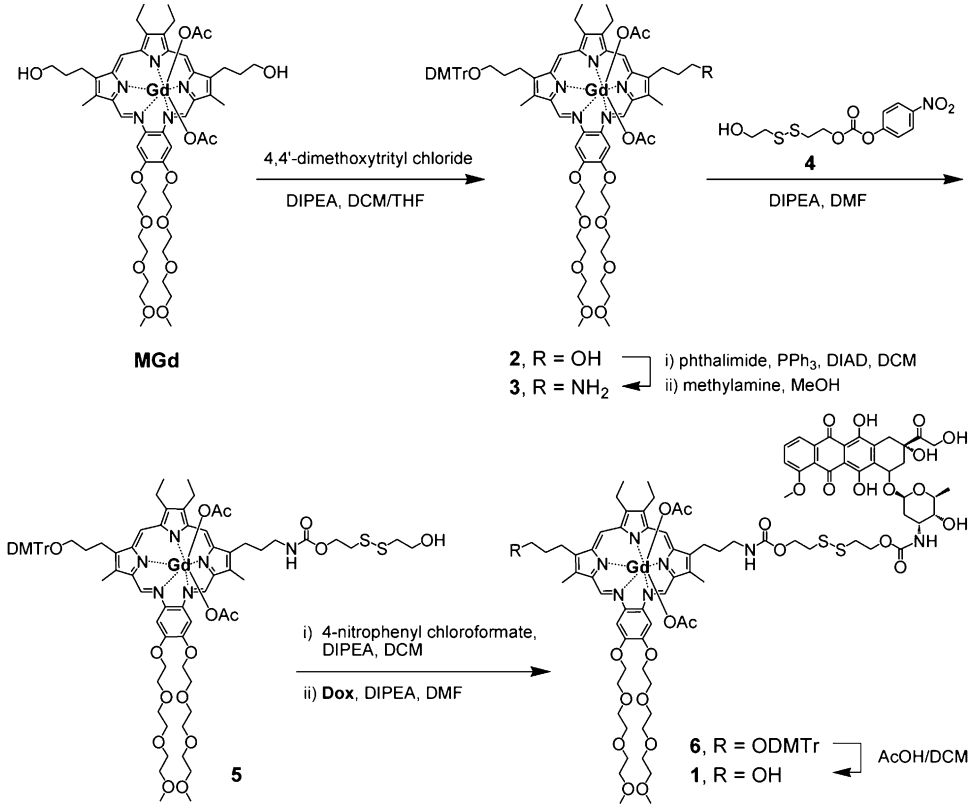

[a]DIPEA = *N*,*N*-diisopropyethylamine; DIAD = diisopropyl azodicarboxylate; Dox = doxorubicin; DMTr = dimethoxytrityl.

theranostics we have developed have been composed of a fluorescent reporter, a cleavable linker, a prodrug, and a tumor-guiding ligand. The cleavable linker is typically chosen to undergo scission upon exposure to the cancer environment (high levels of biomolecules present in cancer cells, relatively low pH, etc.). This releases the active drug agent and in the case of the most effective systems leads to a readily visualized enhancement in the fluorescence emission intensity.

In addition to our theranostic development work, we have studied derivatives of a water-soluble Gd^{3+}-texaphyrin complex known as motexafin gadolinium (**MGd**). The ability of **MGd** to localize preferentially to cancerous lesions has been validated in both clinical models and preclinical studies through inter alia magnetic Gd^{3+} T_1-enhanced MRI and tissue-specific HPLC analyses.[16−22] Recently, this core has been used to create conjugates designed to deliver active platinum species to cancer cells.[23−26] The use of **MGd** to create new theranostic agents is attractive because it permits localization to be monitored by MRI imaging.[27] However, the paramagnetic nature of the coordinated Gd^{3+} center has so far precluded the use of **MGd**-derived systems for fluorescence-based imaging. We considered that by combining a gadolinium texaphyrin core with a potentially fluorescent prodrug via a cleavable linker it might be possible to overcome this deficiency.[28] In principle, this would provide a class of theranostics that could be imaged via two complementary techniques, namely, MRI and fluorescence imaging. Using an active cytotoxin as the fluorophore might permit easy-to-monitor dual mode imaging with a therapeutic benefit thus providing a new class of theranostics suitable for use as, e.g., anticancer agents.

With the above goals in mind, we have designed a new theranostic agent, **1**, wherein a Gd^{3+}-texaphyrin core is conjugated to a doxorubicin prodrug via a disulfide bond. Doxorubicin (Dox) is a frontline cancer chemotherapeutic that is highly fluorescent in aqueous solution. However, as illustrated in Scheme 1 and discussed further below, conjugate **1** exhibits a very weak emission signal, presumably reflecting the fact that the fluorescence of the tethered doxorubicin subunit is quenched by the paramagnetic Gd^{3+}-texaphyrin core. Upon cleavage of the disulfide bond by cellular thiols, a cytotoxic doxorubicin is released. This restores its intrinsic fluorescence and provides for an active cytotoxic agent. Moreover, as expected, the presence of the Gd^{3+}-texaphyrin allows for T_1 contrast enhanced MR imaging in both the intact and cleaved forms. Thus, the selective cellular uptake and subsequent release of doxorubicin by **1** may be readily monitored via a combination of MR imaging and fluorescence turn-on enhancement.

To improve the solubility of conjugate **1** and permit assessment of its utility in vivo, it was loaded into folate-receptor-targeted liposomes. The resulting constructs are termed **FL-1** (folate liposome loaded with **1**). It was expected that **FL-1** would be characterized by prolonged blood circulation times, enhanced solubility relative to that of **1** alone, and improved cancerous tissue targeting.[29−31]

It is well-known that folate receptors are overexpressed on the surface of specific cancer cells,[29] whereas appropriately sized

DOI: 10.1021/jacs.6b09713
J. Am. Chem. Soc. 2016, 138, 16380−16387

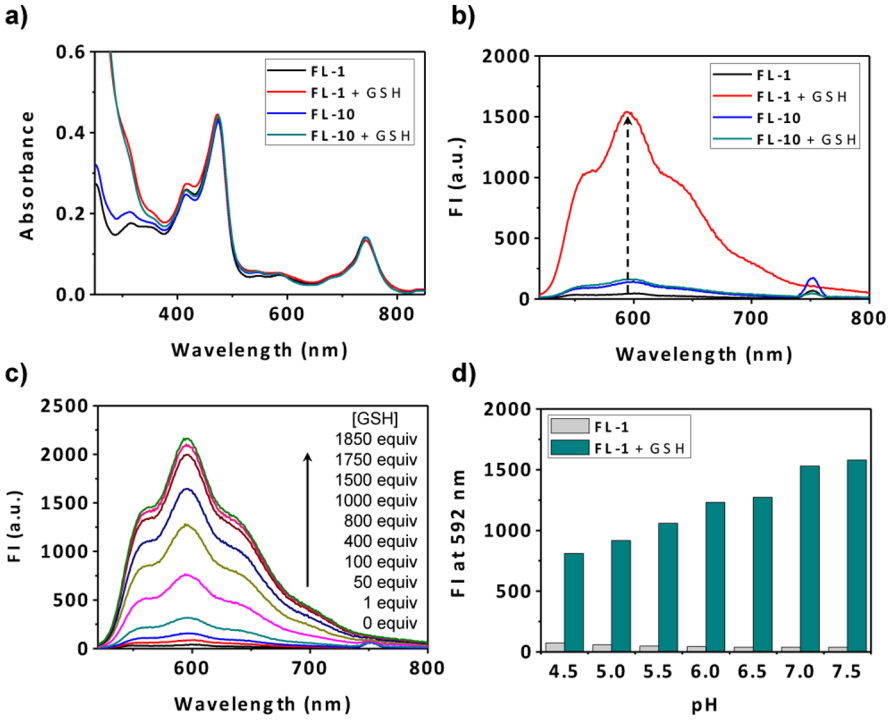

Figure 1. (a) Absorption and (b) fluorescence spectra of **FL-1** and **FL-10** (5 μM, respectively) recorded in the absence and presence of GSH (5 mM) in PBS buffer (10 mM, pH 7.4). (c) Fluorescence spectra of **FL-1** (5 μM) recorded in the presence of different concentrations of GSH in PBS buffer (10 mM, pH 7.4). (d) Fluorescence intensity (FI) at 592 nm determined in the absence and presence of GSH (5 mM) at different pH values. All measurements were made at 37 °C using an excitation wavelength of 500 nm.

liposomes are often taken up well by cancerous lesions as the result of an enhanced permeability and retention (EPR) effect.[30,31] Thus, as illustrated in Scheme 1, it was expected that after injection **FL-1** would enter cancer cells via a combination of EPR localization and folate-receptor-mediated endocytosis. Cancer-enhanced disulfide cleavage[13−15] would then serve to release the active doxorubicin from the **FL-1** while providing a turn-on fluorescent signal.

To test this hypothesis, a variety of in vitro and in vivo studies were carried out using the KB and CT26 (folate-receptor-positive) and HepG2 and NIH3T3 (folate-receptor-negative) cell lines (vide infra). For the sake of comparison, we prepared liposome **L-1** that lacks a folate-receptor-targeting moiety and **FL-10** wherein the S−S bond in the incorporated MGd-Dox conjugate is replaced by a C−C bond.

RESULTS AND DISCUSSION

Conjugate **1** is comprised of doxorubicin (Dox), an antitumor inhibitor of topoisomerase II, a disulfide linker that is readily cleaved by thiols such as glutathione (GSH) that are relatively abundant in tumor cells, and a Gd^{3+}-texaphyrin complex, which serves as an MRI contrast agent. It was prepared according to the synthetic route outlined in Scheme 2. Briefly, **MGd** was converted to monoamino derivative **3** via **2** in accord with previously published procedures.[21] Precursor **3** was then reacted with the disulfide linker component, **4**, in the presence of DIPEA to give **5**, which was then treated with 4-nitrophenyl chloroformate and DIPEA, followed by doxorubicin (Dox) and DIPEA in DMF, to produce **6**. Acid-mediated deprotection then gave texaphyrin−disulfide−doxorubicin conjugate **1**. Texaphyrin−doxorubicin conjugate **10**, containing a CH_2CH_2 bridge instead of the disulfide linker, was prepared using a similar synthetic approach (Scheme S1). All new compounds were characterized by HPLC and ESI mass spectrometry; diamagnetic compounds were further analyzed by ^1H and ^{13}C NMR spectroscopy (Figures S14−S31).

Once in hand, conjugate **1** was converted to a liposomal formulation by mixing with polyethylene glycol-cholesterol (PEG-cholesterol), 1,2-dioleoyl-*sn*-glycero-3-phosphoethanolamine (DOPE), 1,2-dioleoyl-*sn*-glycero-3-phosphoethanolamine-*N*-[methoxy(polyethylene glycol)-2000] (mPEG-DSPE), and 1,2-distearoyl-*sn*-glycero-3-phosphoethanolamine-*N*-[folate(polyethylene glycol)-2000] (folate-PEG-DSPE) at a molar ratio of 4.00:1.00:3.00:1.96:0.04. Evaporation, rehydration with 10 mM HEPES buffer, vortexing, and sonication for 10 min then yielded **FL-1**.

A reference liposomal formulation, **FL-10**, made from control system **10**, was produced in a similar way (cf. Scheme S2). Another control formulation without a folate moiety, **L-1**, was prepared. It consisted of conjugate **1**, PEG-cholesterol, DOPE, and mPEG-DSPE at a molar ratio of 4.00:1.00:3.00:2.00. On the basis of dynamic light scattering studies, the size of **FL-1** was determined to be 31.13 ± 9.10 nm with a −1.02 mV zeta-potential (Figure S1 and Table S1).

Evidence of GSH-induced cleavage came from fluorescence studies carried out in PBS (pH 7.4) at 37 °C. As can be seen from an inspection of Figure 1a, **FL-1** displays a very weak fluorescence. However, when exposed to excess GSH (up to 1500 equiv) a ca. 38-fold increase in the fluorescence intensity at 592 nm is observed. This enhancement proved rather insensitive to pH over the pH range of 4.5−7.5. Analogous optical changes were seen for prodrug **1** under similar conditions (Figures S2−S6).[14,15] No appreciable changes were seen for either **FL-10** or the control conjugate **10** when subject to identical testing. Further evidence for disulfide cleavage in the case of **1** came from HPLC and LC-mass

DOI: 10.1021/jacs.6b09713
J. Am. Chem. Soc. 2016, 138, 16380−16387

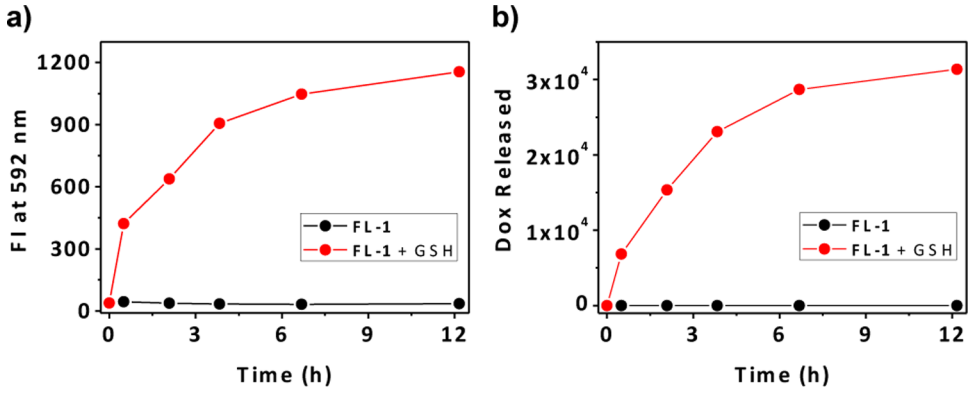

Figure 2. (a) Fluorescence response of **FL-1** (5 μM) with and without GSH (5 mM). Excitation was effected at 500 nm. (b) Dox released from **FL-1** (5 μM) as a function of time in the presence and absence of GSH (5 mM). Dox in HPLC chromatograms was detected by UV/vis absorption using 500 nm as the interrogation wavelength. All data were recorded in PBS buffer (10 mM, pH 7.4) at 37 °C.

spectrometry experiments (Figure S7). A proposed mechanism for the GSH-induced disulfide cleavage is shown in Scheme S3.

Further confirmation that release of free Dox occurs upon disulfide bond cleavage came from combined HPLC and fluorimetric time-dependent analyses of **FL-1** (Figure 2). Upon treating **FL-1** with GSH, the amount of Dox released was found to correlate with the observed increase in fluorescence intensity at 592 nm (arising from free Dox). In contrast, in the absence of GSH, little evidence of Dox release was seen by HPLC nor was an enhancement in the fluorescence intensity at 592 nm observed over the full 12 h time course of the experiment. Similar observations were made in the case of the prodrug conjugate **1** (cf. Figure S8). We thus consider that the fluorescence changes at 592 nm provide an off–on signal that may be used to follow directly Dox release.

As the result of its folate-functionalized PEGylated liposomal formulation, **FL-1** was expected to provide for the tumor-targeted delivery of Dox via receptor-mediated endocytosis. Tests of this expectation were carried out using the KB and CT26 cell lines, which express folate receptors on the cell surface, as well as the HepG2 and NIH3T3 cell lines, which are folate-receptor-deficient. When the cells were treated with 4 μM of **FL-1** for 1 h, strong fluorescence signals were observed in the folate-receptor-positive cells, KB and CT26. In contrast, only a very weak fluorescence signal was seen in the case of the HepG2 and NIH3T3 cells (Figure 3). Support for the enhanced uptake via folate receptor targeting inferred from these optical studies came from histogram plots and quantitative fluorescence intensity measurements carried out via flow cytometry (Figure S9). Control liposomes (**L-1**), containing **1** but lacking the folate moieties, were then made up. They were applied to the folate-receptor-expressing KB and CT26 cells in direct analogy to what was done in the case of **FL-1**. In this case, considerably lower levels of Dox uptake were observed, as inferred from comparative fluorescent microscopic imaging (cf. Figure S10). On the basis of these results, we conclude that **FL-1** permits the active targeted delivery of **1** into cancerous cells overexpressing the folate receptor and that Dox is released effectively within these cells.

The in vitro anticancer effects of **FL-1** were examined using standard MTT cell viability assays. Significant and moderate antiproliferative activity was seen at 5 μM in the case of the KB and CT26 cell lines, respectively. Dose-dependent effects were seen, with the activity increasing with concentration. At all concentrations, the activity was lower in the case of the HepG2

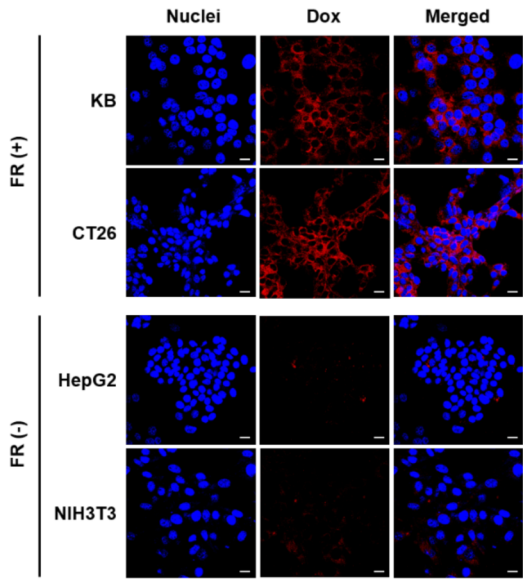

Figure 3. Fluorescence images of **FL-1**-treated cells. Folate receptor positive (KB, CT26) and negative (HepG2, NIH3T3) cell lines were treated with 4 μM of **FL-1** for 1 h. The cells were then fixed in 4% paraformaldehyde after washing with PBS, and then stained with Hoechst (nuclear counterstain, blue). Scale bar: 20 μm.

and NIH3T3 cell lines lacking the overexpressed folate receptors present in the KB and CT26 cell lines (Figure 4).

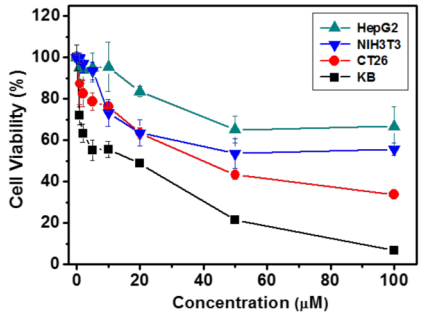

Figure 4. Antiproliferative activity of **FL-1** in various cell lines as inferred from MTT assays. Folate receptor positive (KB, CT26) and negative (HepG2, NIH3T3) cell lines were treated with various concentration of **FL-1** for 48 h prior to analysis.

DOI: 10.1021/jacs.6b09713
J. Am. Chem. Soc. 2016, 138, 16380–16387

However, the free Dox control showed approximately similar anticancer activity in both the KB and HepG2 cell lines and has activity regardless of whether a folate receptor is present in the liposome (Figure S11). The antiproliferative activity of **FL-1** is expected to reflect both liposome-based folate receptor targeting and Dox release via disulfide bond reduction. To test the importance of the latter factor, we prepared **FL-10**, a folate-receptor-targeted liposomal formulation loaded with control compound **10** containing a CH_2CH_2 unit instead of the S−S linker present in **1**. Treatment of folate-receptor-positive cell lines KB and CT26 with this liposomal formulation resulted in a considerably lower antiproliferative effect than that seen for **FL-1** (Figure S12 and Table S2). The MTT assay results were supported by fluorescence measurements that revealed an increase in the Dox-based emission intensity. We thus believe that the disulfide bond present in **1** (and **FL-1**) facilitates the release of free Dox.

Conjugate **1** is expected to enhance T_1-weighted MR images through the coordinated Gd^{3+} center present in the texaphyrin core. Therefore, we examined the MR relaxivity of **FL-1** in phosphate-buffered saline (PBS). The T_1 relaxivities of **FL-1** were calculated to be 11.8 ± 0.3 and 7.1 ± 0.4 mM^{-1} s^{-1} at 60 and 200 MHz, respectively (Figure 5a). Phantom images acquired at 200 MHz in PBS reveal increasingly bright signals as the concentration of **FL-1** increases (Figure 5b).

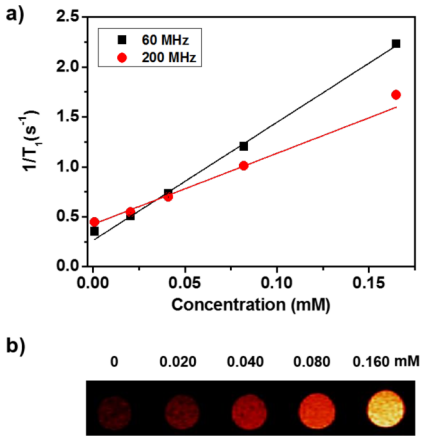

Figure 5. (a) T_1 relaxivity measurements of **FL-1** in PBS solution as a function of concentrations at 60 and 200 MHz. (b) T_1-weighted spin−echo MR phantom images recorded at different concentrations of **FL-1**.

We also confirmed that pellets of KB cells treated with ≥10 μM concentrations of **FL-1** could be visualized by fluorescence emission as well as by use of an MRI scanner (Figure S13). These results are taken as evidence that **FL-1** would provide sufficient T_1 relaxivity to enable MR visualization in vivo and that, upon linker scission, would allow based Dox fluorescence-based imaging.

As a test of the above hypothesis, two different cancer mouse models, consisting of a metastatic liver cancer orthotropic model and a subcutaneous (s.c.) KB cell xenograft model, were used. First, we evaluated whether **FL-1** would accumulate in the tumor site and induce tumor regression in the s.c. xenograft nude mouse model. Liposome **L-1** contains **1** but lacks folate-receptor-targeting moieties; it was also used as a control. Here, whole-body fluorescence imaging revealed a strong, tumor-localized signal 6 h after **FL-1** was administered intravenously via tail vein injection (Figure 6a). Cryo-sectioned tumor sections of animals treated with **FL-1** were monitored after 24 h using confocal microscopy; again, strong enhancement was seen. In contrast, in the case of **L-1** a viable fluorescence signal was rarely seen (Figure 6b). Furthermore, good signal-to-noise ratios (SNRs) were seen for tumor tissues under conditions of T_1 MR imaging (Figure 6c). The inferred localization provides a rationale for the relative reduction in tumor burden seen for **FL-1** versus that of saline control as determined from time-dependent tumor size measurements (Figure 6d).

The metastatic liver cancer model used for this study was obtained via the intrasplenic administration of CT26 cells to nude mice. Enhanced MR signals ascribed to **FL-1** were seen in the tumor region as early as 30 min after intravenous administration (tail vein injection). This stands in contrast to what was seen in the case of **L-1**. The intensity of the signal decreased only gradually with time, presumably reflecting slow clearance of the conjugate from the tumor site (Figure 7a). As inferred from T_1-weighted MR images (Figure 7b), **FL-1** effectively reveals the tumor area which is surrounded by normal liver tissue and can do so at an early stage of metastatic disease (3 days postinoculation).

To assess therapeutic efficacy in the metastatic liver cancer model, **FL-1** (2.5 mg/kg) was administered intravenously in form of four doses. These doses were administered once every other day starting on day 3 after inoculation with the CT26 cells used to produce the model. The extent of metastasis was monitored weekly starting at 7 days post inoculation using T_2-weighted MR imaging (Figure 8). In all cases, a bright spot was seen at day 7 by T_2-weighted MRI, a finding ascribed to the initial migration of CT26 cells from the spleen into the liver. One week later, MR imaging revealed metastatic tumors scattered throughout the liver, with the extent of this dissemination being considerably greater in the case of the saline control (Figure 8a). By day 21, the liver appeared fully invaded in the case of the saline control, whereas the metastases remained localized in the case of **FL-1**.

The survival rates of the saline control, the **FL-10** control, and the **FL-1**-treated group were compared using the metastatic liver model mice. A Kaplan−Meier analysis was carried out and revealed that the cumulative survival rates were enhanced for **FL-1** relative to both the saline control and **FL-10**. No mice treated with saline survived past day 45. However, at that time (i.e., day 45 post inoculation) 37.5% of the mice treated with **FL-1** were still alive. By day 60, none of the **FL-10** treated animals were alive, whereas several treated with **FL-1** were (see Figure 8b).

■ CONCLUSIONS

We have described the synthesis, spectroscopic properties, target-specific internalization, and therapeutic effects of conjugate **1** and liposomal formulation **FL-1** as theranostic agents. The choice of components, namely, a Gd^{3+}-texaphyrin core conjugated to a doxorubicin prodrug via a disulfide bond, allows for dual modality imaging as well as therapy in mice models. The use of folate-receptor-targeting liposomes permits enhanced tumor uptake. GSH-mediated cleavage of the disulfide linker leads to release of free doxorubicin coupled with a fluorescence increase at 592 nm. Enhanced imaging, as well as antiproliferative effects, were seen in the folate-receptor positive cell lines, KB and CT26, relative to that in the folate-receptor negative cell lines, HepG2 and NIH3T3. The present system, **FL-1**, permits enhanced MR imaging in vivo under

DOI: 10.1021/jacs.6b09713
J. Am. Chem. Soc. 2016, 138, 16380−16387

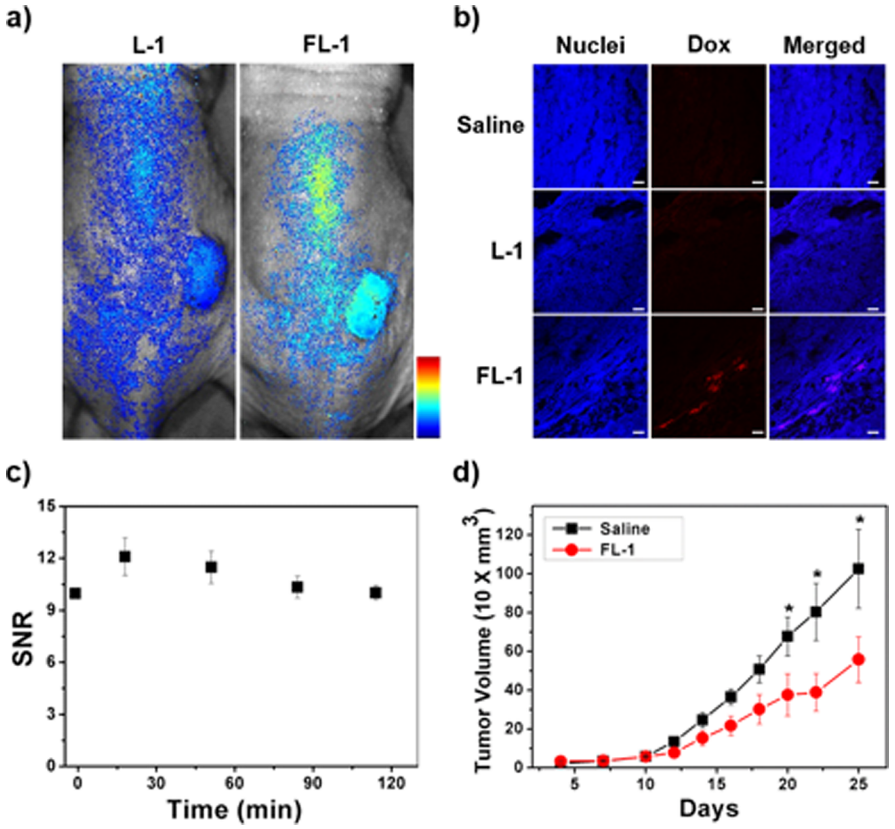

Figure 6. (a) Whole-body in vivo fluorescence images recorded 6 h after intravenous injection of **L-1** or **FL-1** to nude mice bearing KB cell-derived tumors (s.c. xenograft model). (b) Fluorescence microscopy images of cryo-sectioned tumor tissues taken from the s.c. xenograft animals 24 h after **L-1** or **FL-1** administration. (c) Signal-to-noise ratio (SNR) for MR images of the tumor tissue for this same model. (d) Tumor volume vs time for s.c. xenograft mice treated with saline and **FL-1** (Mean ± SEM, $n = 4$, *, $p < 0.05$, Student's t test).

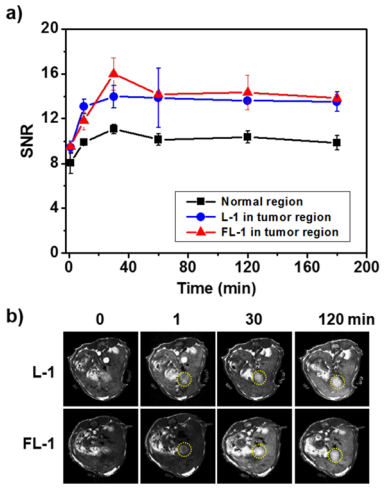

Figure 7. (a) Comparison of signal-to-noise ratio (SNR) between normal and tumorous regions in liver tissues treated with **L-1** or **FL-1**. (b) T_1-weighted MR images of **L-1** and **FL-1** that were tested for the early diagnosis of metastatic liver cancer in mice models. Yellow circles indicate the metastatic tumor regions.

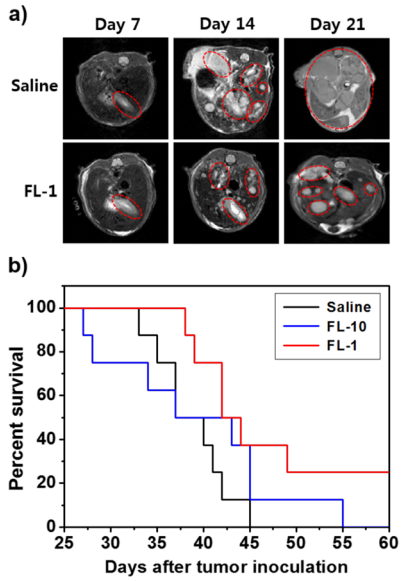

Figure 8. (a) T_2-weighted MR images showing the livers of nude mice recorded at the indicated times postinoculation with CT26 cells (metastatic liver cancer model). Red circles indicated the metastatic tumors. (b) Kaplan–Meier curves showing the cumulative survival rates of metastatic liver model mice after injection with saline (black line), **FL-10** (blue line), or **FL-1** (red line). Survival was enhanced for **FL-1** relative to the saline control or **FL-10**.

conditions of T_1 contrast, allowing the progression of metastatic cancer to be followed in vivo during its early stages. Finally, time-dependent tumor regrowth studies revealed that **FL-1** is capable of reducing the tumor burden in both subcutaneous and metastatic liver cancer mouse models. On the basis of the findings presented here we propose that conjugates such as **1** and its liposomal formulation **FL-1** which permit dual imaging and provide a therapeutic potential may have an important role to play as theranostics particularly for

DOI: 10.1021/jacs.6b09713
J. Am. Chem. Soc. 2016, 138, 16380–16387

the early diagnosis and treatment of metastatic liver cancer. Efforts to develop such agents are thus ongoing.

■ ASSOCIATED CONTENT

Supporting Information

The Supporting Information is available free of charge on the ACS Publications website at DOI: 10.1021/jacs.6b09713.

Synthetic and spectroscopic methods, additional spectra (UV/vis absorption, fluorescence, NMR, and ESI-MS) and imaging data and full reference information (PDF)

■ AUTHOR INFORMATION

Corresponding Authors

*E-mail: minheelee@sookmyung.ac.kr.
*E-mail: kshong@kbsi.re.kr.
*E-mail: jongskim@korea.ac.kr.
*E-mail: sessler@cm.utexas.edu.

ORCID

Jonathan L. Sessler: 0000-0002-9576-1325

Author Contributions

M.H.L. and E.J.K. contributed equally to this study.

Notes

The authors declare no competing financial interest.

■ ACKNOWLEDGMENTS

This research was supported by the Korean National Research Foundation (NRF) (2015R1C1A2A01054496, M.H.L; CRI 2009-0081566, J.S.K), the Korea Basic Science Institute (D35401, K.S.H), the R&D Convergence Program (CRC-15-02-KRIBB, K.S.H) of NST (National Research Council of Science & Technology) of the Republic of Korea, and the National Institutes of Health (CA68682, J.L.S).

■ REFERENCES

(1) Sleeman, J.; Steeg, P. S. *Eur. J. Cancer* **2010**, *46*, 1177−1180.
(2) Steeg, P. S. *Nat. Rev. Cancer* **2016**, *16*, 201−218.
(3) Namasivayam, S.; Martin, D. R.; Saini, S. *Cancer Imaging* **2007**, *7*, 2−9.
(4) Imam, K.; Bluemke, D. A. *Magn. Reson. Imaging Clin. N. Am.* **2000**, *8*, 741−756.
(5) Schima, W.; Kulinna, C.; Langenberger, H.; Ba-Ssalamah, A. *Cancer Imaging* **2005**, *5*, S149−S156.
(6) Kokudo, N.; Ishizawa, T. *Liver Cancer* **2012**, *1*, 15−21.
(7) Shimada, S.; Ohtsubo, S.; Ogasawara, K.; Kusano, M. *World J. Surg. Oncol.* **2015**, *13*, 198−206.
(8) Verwilst, P.; Park, S.; Yoon, B.; Kim, J. S. *Chem. Soc. Rev.* **2015**, *44*, 1791−1806.
(9) Kim, E.-J.; Bhuniya, S.; Lee, H.; Kim, H. M.; Shin, W. S.; Kim, J. S.; Hong, K. S. *ACS Appl. Mater. Interfaces* **2016**, *8*, 10266−10273.
(10) Vivero-Escoto, J. L.; Huxford-Phillips, R. C.; Lin, W. *Chem. Soc. Rev.* **2012**, *41*, 2673−2685.
(11) Shanmugam, V.; Selvakumar, S.; Yeh, C. S. *Chem. Soc. Rev.* **2014**, *43*, 6254−6287.
(12) Bardhan, R.; Lal, S.; Joshi, A.; Halas, N. J. *Acc. Chem. Res.* **2011**, *44*, 936−946.
(13) Kumar, R.; Shin, W. S.; Sunwoo, K.; Kim, W. Y.; Koo, S.; Bhuniya, S.; Kim, J. S. *Chem. Soc. Rev.* **2015**, *44*, 6670−6683.
(14) Lee, M. H.; Sessler, J. L.; Kim, J. S. *Acc. Chem. Res.* **2015**, *48*, 2935−2946.
(15) Lee, M. H.; Han, J. H.; Kim, J. Y.; Bhuniya, S.; Sessler, J. L.; Kang, C.; Kim, J. S. *J. Am. Chem. Soc.* **2012**, *134*, 12668−12674.
(16) Preihs, C.; Arambula, J. F.; Magda, D.; Jeong, H.; Yoo, D.; Cheon, J.; Siddik, Z. H.; Sessler, J. L. *Inorg. Chem.* **2013**, *52*, 12184−12192.
(17) Young, S. W.; Qing, F.; Harriman, A.; Sessler, J. L.; Dow, W. C.; Mody, T. D.; Hemmi, G. W.; Hao, Y.; Miller, R. A. *Proc. Natl. Acad. Sci. U. S. A.* **1996**, *93*, 6610−6615.
(18) Sessler, J. L.; Mody, T. D.; Hemmi, G. W.; Lynch, V.; Young, S. W.; Miller, R. A. *J. Am. Chem. Soc.* **1993**, *115*, 10368−10369.
(19) Mehta, M. P.; Shapiro, W. R.; Phan, S. C.; Gervais, R.; Carrie, C.; Chabot, P.; Patchell, R. A.; Glantz, M. J.; Recht, L.; Langer, C.; Sur, R. K.; Roa, W. H.; Mahe, M. A.; Fortin, A.; Nieder, C.; Meyers, C. A.; Smith, J. A.; Miller, R. A.; Renschler, M. F. *Int. J. Radiat. Oncol., Biol., Phys.* **2009**, *73*, 1069−1076.
(20) Patel, H.; Mick, R.; Finlay, J.; Zhu, T. C.; Rickter, E.; Cengel, K. A.; Malkowicz, S. B.; Hahn, S. M.; Busch, T. M. *Clin. Cancer Res.* **2008**, *14*, 4869−4876.
(21) Wei, W.-H.; Fountain, M.; Magda, D.; Wang, Z.; Lecane, P.; Mesfin, M.; Miles, D.; Sessler, J. L. *Org. Biomol. Chem.* **2005**, *3*, 3290−3296.
(22) Miles, D. R.; Mesfin, M.; Mody, T. D.; Stiles, M.; Lee, J.; Fiene, J.; Denis, B.; Boswell, G. W. *Anal. Bioanal. Chem.* **2006**, *385*, 345−356.
(23) Arambula, J. F.; Sessler, J. L.; Siddik, Z. H. *Bioorg. Med. Chem. Lett.* **2011**, *21*, 1701−1705.
(24) Arambula, J. F.; Sessler, J. L.; Siddik, Z. H. *MedChemComm* **2012**, *3*, 1275−1281.
(25) Thiabaud, G.; Arambula, J. F.; Siddik, Z. H.; Sessler, J. L. *Chem. - Eur. J.* **2014**, *20*, 8942−8947.
(26) Thiabaud, G.; McCall, R.; He, G.; Arambula, J. F.; Siddik, Z. H.; Sessler, J. L. *Angew. Chem., Int. Ed.* **2016**, *55*, 12626−12631.
(27) Barkey, N. M.; Preihs, C.; Cornnell, H. H.; Martinez, G.; Carie, A.; Vagner, J.; Xu, L.; Lloyd, M. C.; Lynch, V. M.; Hruby, V. J.; Sessler, J. L.; Sill, K. N.; Gillies, R. J.; Morse, D. L. *J. Med. Chem.* **2013**, *56*, 6330−6338.
(28) Lee, M. H.; Kim, E.-J.; Lee, H.; Park, S. Y.; Hong, K. S.; Kim, J. S.; Sessler, J. L. *Chem. Commun.* **2016**, *52*, 10551−10554.
(29) Low, P. S.; Henne, W. A.; Doorneweerd, D. D. *Acc. Chem. Res.* **2008**, *41*, 120−129.
(30) Sykes, E. A.; Chen, J.; Zheng, G.; Chan, W. C. *ACS Nano* **2014**, *8*, 5696−5706.
(31) Wang, J.; Mao, W.; Lock, L. L.; Tang, J.; Sui, M.; Sun, W.; Cui, H.; Xu, D.; Shen, Y. *ACS Nano* **2015**, *9*, 7195−7206.